Imaging Science in Dentistry 2020; 50: 199-208
https://doi.org/10.5624/isd.2020.50.3.199

In vivo quantification of mandibular bone remodeling and vascular changes in a Wistar rat model: A novel HR-MRI and micro-CT fusion technique

Dandan Song[1], Sohaib Shujaat[1], Ruiting Zhao[1], Yan Huang[1], Eman Shaheen[1], Jeroen Van Dessel[1], Kaan Orhan[1,2], Greetje Vande Velde[3], Ruxandra Coropciuc[1], Ruben Pauwels[1,4,5], Constantinus Politis[1], Reinhilde Jacobs[1,6,*]

[1]*OMFS IMPATH Research Group, Department of Imaging and Pathology, Faculty of Medicine, KU Leuven and Oral and Maxillofacial Surgery, University Hospitals Leuven, Leuven, Belgium*
[2]*Department of Dentomaxillofacial Radiology, Faculty of Dentistry, University of Ankara, Ankara, Turkey*
[3]*Biomedical MRI, Department of Imaging and Pathology, Faculty of Medicine, KU Leuven, Leuven, Belgium*
[4]*Department of Radiology, Faculty of Dentistry, Chulalongkorn University, Bangkok, Thailand*
[5]*Aarhus Institute of Advanced Studies, Aarhus University, Aarhus, Denmark*
[6]*Department of Dental Medicine, Karolinska Institute, Stockholm, Sweden*

ABSTRACT

Purpose: This study was performed to introduce an *in vivo* hybrid multimodality technique involving the co-registration of micro-computed tomography (micro-CT) and high-resolution magnetic resonance imaging (HR-MRI) to concomitantly visualize and quantify mineralization and vascularization at follow-up in a rat model.

Materials and Methods: Three adult female rats were randomly assigned as test subjects, with 1 rat serving as a control subject. For 20 weeks, the test rats received a weekly intravenous injection of 30 μg/kg zoledronic acid, and the control rat was administered a similar dose of normal saline. Bilateral extraction of the lower first and second molars was performed after 10 weeks. All rats were scanned once every 4 weeks with both micro-CT and HR-MRI. Micro-CT and HR-MRI images were registered and fused in the same 3-dimensional region to quantify blood flow velocity and trabecular bone thickness at T0 (baseline), T4 (4 weeks), T8 (8 weeks), T12 (12 weeks), T16 (16 weeks), and T20 (20 weeks). Histological assessment was the gold standard with which the findings were compared.

Results: The histomorphometric images at T20 aligned with the HR-MRI findings, with both test and control rats demonstrating reduced trabecular bone vasculature and blood vessel density. The micro-CT findings were also consistent with the histomorphometric changes, which revealed that the test rats had thicker trabecular bone and smaller marrow spaces than the control rat.

Conclusion: The combination of micro-CT and HR-MRI may be considered a powerful non-invasive novel technique for the longitudinal quantification of localized mineralization and vascularization. ***(Imaging Sci Dent 2020; 50: 199-208)***

KEY WORDS: Vascular Remodeling; Radiology; Jaw; Rats

Introduction

Bone is a highly vascularized feedback-controlled composite organ that fulfills several interconnected functions, including locomotion, phosphate and calcium metabolism, the synthesis of endocrine molecules, and hematopoiesis.[1-3] It is a dynamic tissue that is continuously being modeled and remodeled to maintain the integrity of the skeletal

The project was supported by the China Scholarship Council (No. 201708210187). Ruben Pauwels is supported by the European Union Horizon 2020 Research and Innovation Programme under the Marie Skłodowska-Curie grant agreement number 754513 and by the Aarhus University Research Foundation (AIAS-COFUND).
Received March 2, 2020; Revised June 7, 2020; Accepted June 25, 2020
*Correspondence to : Prof. Reinhilde Jacobs
OMFS IMPATH Research Group, Department of Imaging and Pathology, Katholieke University Leuven, Campus Sint-Rafael, Kapucijnenvoer 33, 3000 Leuven, Belgium
Tel) 32-16332452, E-mail) reinhilde.jacobs@kuleuven.be

Imaging Science in Dentistry · pISSN 2233-7822 eISSN 2233-7830

structure via the regulated activity of osteoblast and osteoclast cells.[4-6]

The preferred method for the assessment of bone and vascular microstructure includes 2-dimensional histological sections,[7] micro-computed tomography (micro-CT) imaging with or without contrast agents, and laser Doppler flowmetry.[8-10] Histomorphology has been considered the gold standard for identifying and visualizing the microstructure of bone and blood vessels; however, it is an invasive and time-consuming procedure and is associated with random sampling errors.[11] Similarly, micro-CT with or without contrast agents is a powerful non-invasive technique for the visualization of bone and vascular microstructure in 3 dimensions, but it cannot be used for hemodynamic analysis.[12,13] Jia et al.[14] and Roche et al.[15] have suggested the application of micro-CT with a barium sulfate contrast agent to characterize and quantify bone remodeling and blood vessel structure. However, this technique can only be used to easily view large vascular structures and cannot visualize vascularity within trabecular bone.[16,17] Recently, high-resolution magnetic resonance imaging (HR-MRI) has been proposed for the quantification of vascularity at the micro-anatomical level, but this technique cannot be used to quantify the bone microstructure.[18,19]

To overcome the aforementioned limitations of individual imaging modalities, various co-registered hybrid multimodal imaging techniques have been suggested to offer more accurate and detailed insight into the physiology of bone and its associated vasculature compared to the assessment of separate images. Methods such as the co-registration of micro-CT/micro-positron emission tomography,[20,21] micro-CT/single-photon emission computed tomography,[22] micro-CT/MRI,[23] CT/MRI,[24] dynamic contrast-enhanced CT/MRI,[25] and micro-digital subtraction angiography/MRI[26] have been proposed to offer better insight into the physiological processes of bone remodeling, angiogenesis, and blood flow. However, the potential of co-registered intermodal imaging for the assessment of bone structure and microvascularization at follow-up remains unclear, and few studies have been conducted on bone remodeling and blood flow velocity (BFV) at follow-up. Although histomorphometric analysis is usually considered the gold standard, it cannot be used to assess the evolution of bone changes over time unless a multifold sample of animals is utilized. We hypothesized that a combination of micro-CT and HR-MRI could provide a better understanding of the follow-up interaction between angiogenic and osteogenic pathways within a region of interest. As such, the purpose of this study was to introduce an *in vivo* hybrid multimodal technique with co-registered micro-CT/HR-MRI data to concomitantly visualize and quantify bone remodeling and vascularization at follow-up in a rat model.

Materials and Methods

The experimental protocol was approved by the Ethical Committee for Animal Experimentation of KU Leuven in Leuven, Belgium (reference no. P264/2015) and was carried out in accordance with the UK Animals (Scientific Procedures) Act of 1986 and the EU Directive 2010/63/EU for animal experiments.

A sample of 4 female Wistar rats (200-250 g; aged 12 weeks) was obtained. Three adult female rats were randomly assigned as test subjects, and 1 rat was assigned as a control subject. For 20 weeks, the test rats received an intravenous injection of zoledronic acid (ZA; 30 μg/kg per week), while the control rat was intravenously administered normal saline (30 μg/kg per week). At the end of the 10th week, bilateral extraction of the lower first and second molars was performed in each rat under general anesthesia (1.5%-2% isoflurane in 100% oxygen) to simulate a bisphosphonate-related osteonecrosis of the jaw (BRONJ)-associated bone defect.[27,28] Based on the genetic differences between humans and rodents, a 10-week ZA delivery period with the mentioned dosage frequency along with tooth extraction is known to be capable of effectively replicating a BRONJ-associated bone defect.[29] ZA was delivered for an additional 10 weeks after tooth extraction so that follow-up changes in the region of the bone defect could be observed.

Micro-CT acquisition

The rats were anesthetized by placing them in an anesthesia induction chamber, to which isoflurane inhalation anesthesia was delivered at a rate of 5 cc/minute for 3-5 minutes. Following anesthesia, each rat was scanned by placing it on a stable platform with a gas mask on its nose to avoid movement, and a cylindrical plastic holder was applied to immobilize the head. The trabecular bone changes were observed by scanning all rats once every 4 weeks (T0: baseline, T4: 4 weeks, T8: 8 weeks, T12: 12 weeks, T16: 16 weeks, T20: 20 weeks) with a dedicated *in vivo* micro-CT scanner (SkyScan 1076; Bruker microCT, Kontich, Belgium), operating at 80 kV and 120 μA with a 1-mm aluminum filter and a scanning time of approximately 11 minutes. Furthermore, an averaging frame of 6° was

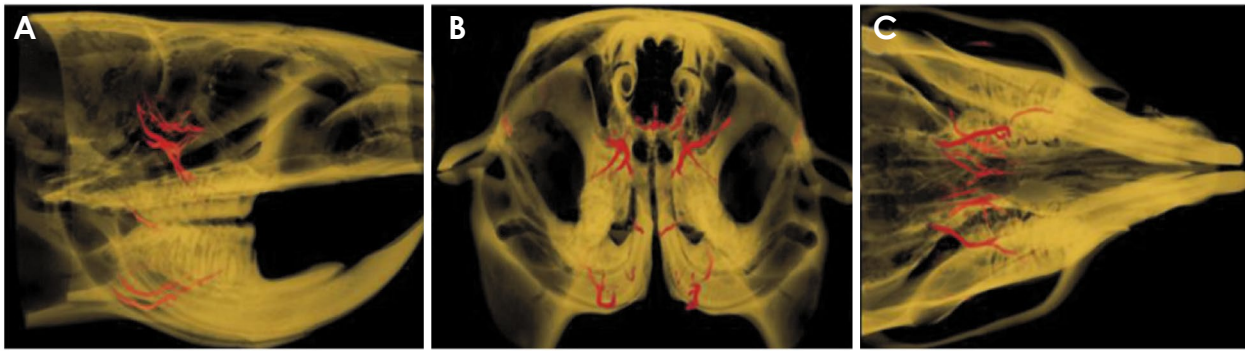

Fig. 1. Registered high-resolution magnetic resonance images and micro-computed tomography images allowing accurate projection of the available blood vessels onto the jaw bone. A. Longitudinal view. B. Coronal view. C. Inferior view.

applied along with a 220° arc of rotation around the vertical axis with a rotation step of 0.8°. With the same settings, bone mineral density phantoms of 0.25 g/cm^3 and 0.75 g/cm^3 were scanned to perform bone mineral density calibration with respect to the attenuation values. The rats were scanned once every 4 weeks to keep the scanning protocol timing consistent and to minimize the impact of radiation on the bone tissue microstructure. Additionally, scanning was carried out 2 weeks after tooth extraction rather than immediately to allow for soft tissue healing over the simulated defect. Following image acquisition, 3-dimensional (3D) datasets with an isotropic voxel size of 35 μm^3 were reconstructed without smoothening and were processed using NRecon software (version 1.6.10.4; Bruker microCT). A beam hardening correction of 30% was applied for image conversion.

HR-MRI acquisition

HR-MRI scanning was performed at the same time points as micro-CT imaging and under a similar anesthetic protocol. To observe the vascular changes, T2-weighted HR-MRI images were acquired utilizing a Biospec 9.4-T small-animal MRI scanner with high resolution (59 × 59 × 59 μm; HR-MRI) (Bruker Biospin, Ettlingen, Germany) with a 20-cm horizontal bore and an actively shielded gradient insert. A cross-coil setup was applied, consisting of a horizontal radio-frequency coil (transmit/receive coil, 7.2-cm diameter; Bruker Biospin) and a rat head surface receiving coil (Rapid Biomedical, Rimpar, Germany). Magnetic resonance angiography (MRA) was performed with a time-of-flight (TOF) 2-dimensional sequence (echo time: 3.5 ms, repetition time: 18 ms, slice thickness: 1 mm, matrix size: 256 × 256, slices: 60, and FOV: 40 × 26 mm), resulting in in-plane resolution 3D T2-weighted anatomical MRI and MRA.

Registration of HR-MRI and micro-CT images

The HR-MRI 3D reconstructed images were spatially aligned with the micro-CT images in the same 3D space using Amira software (version 6.3.0; Thermo Fisher Scientific, Merignac, France). Manual registration was applied to visualize the vascular and skeletal structures in longitudinal (Fig. 1A), coronal (Fig. 1B), and inferior (Fig. 1C) 3D views. Thereafter, the micro-CT and HR-MR images were fused in Synapse 3D® software (Fujifilm Medical, Tokyo, Japan) (Fig. 2) for quantification of rat jawbone remodeling and vascularization. For fusion, a suitable region of interest (ROI) was defined to enable the calculation of vascularity as close as possible to the affected bone. Fusion was carried out separately for each rat at each time point.

Bone morphometric analysis

Following fusion, the micro-CT images were transformed using CT-Analyzer® software (Bruker microCT) for the calculation of morphometric parameters at all-time points. No blurring of the images due to breathing were observed. A volume of interest (VOI) was manually selected to include mandibular alveolar bone bilaterally at the apical region of the first and second molar of each rat while excluding the root surface and mandibular canal (Figs. 3A and B). Later, segmentation within the selected VOI was performed using a global automatic threshold algorithm. The trabecular thickness (Tb.Th; mm) was semi-automatically calculated at all time points before (Figs. 3C and D) and after (Figs. 3E and F) extraction.

BFV analysis

For the quantification of vascular changes, fused micro-CT images and TOF-MRA were used to estimate the relative BFV in the rat mandible as suggested by Huang et al.[30] The closest artery and its branch connected to the

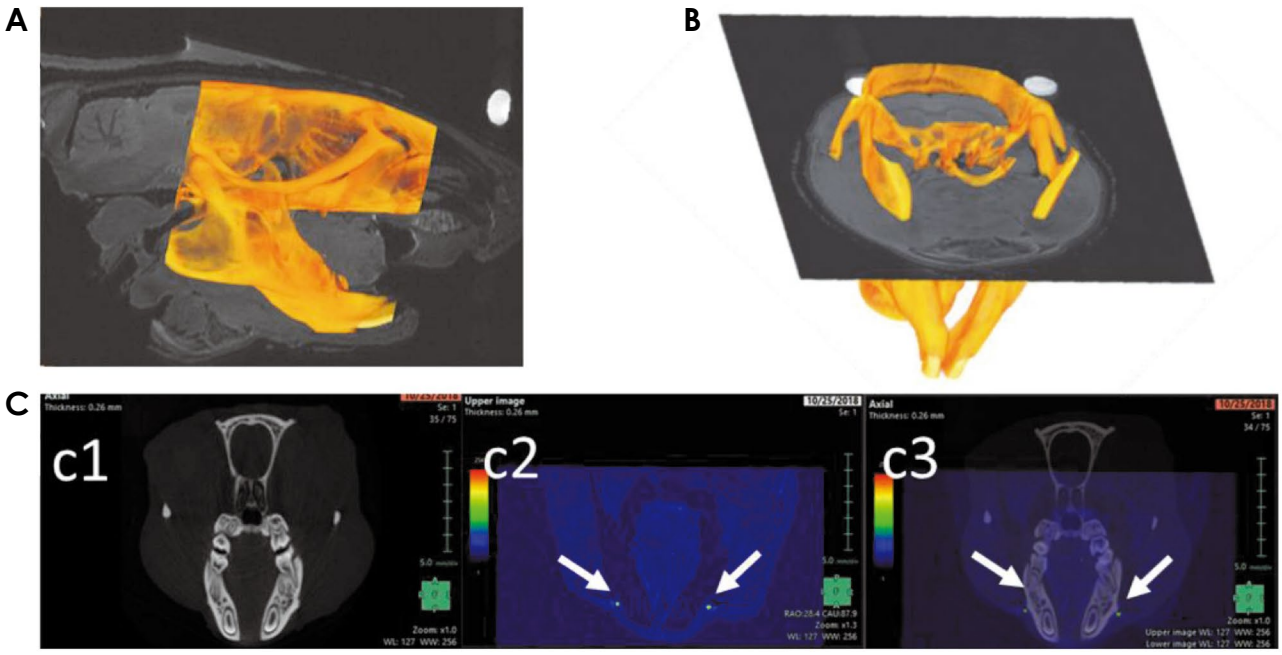

Fig. 2. Combination of micro-computed tomography and high-resolution magnetic resonance imaging (HR-MRI) scans. A. Three-dimensional (3D) sagittal view. B. 3D coronal view (posterior). C. Sample of imaging fusion (c1) hard tissue from micro-CT imaging and (c2) soft tissue from HR-MRI. (c3) Imaging fusion of c1 and c2.

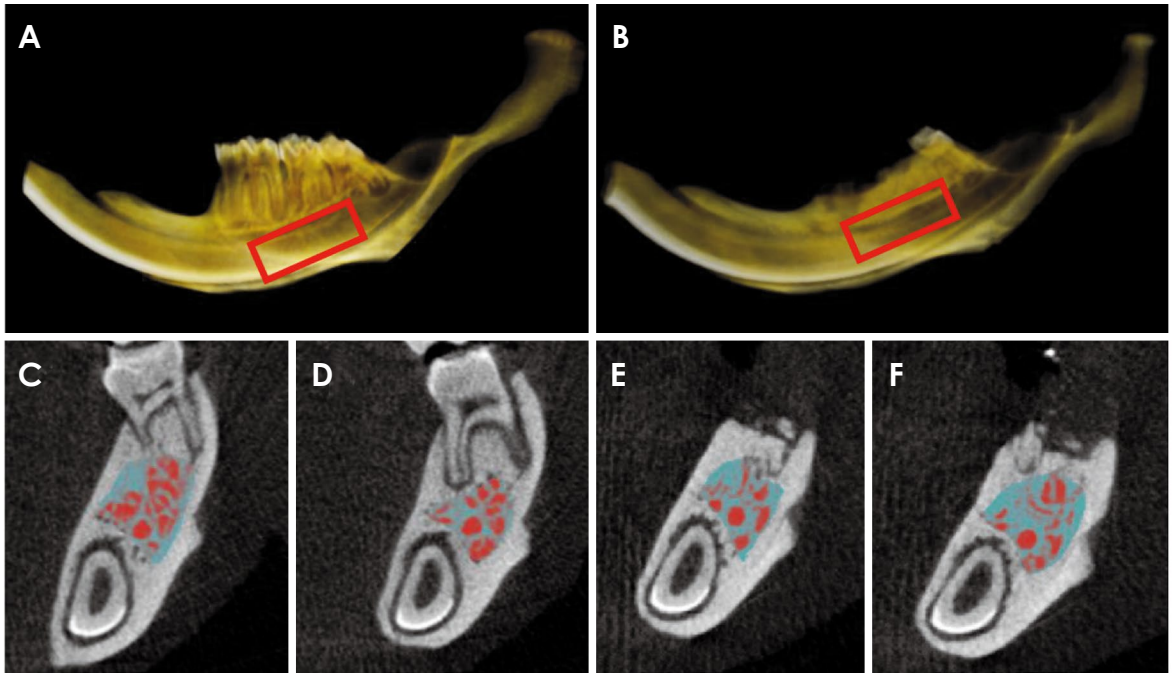

Fig. 3. Example of trabecular bone thickness changes in a test rat. A. Volume of interest (VOI) at the periapical region of the first and second molar. B. VOI following tooth extraction. C, D. Trabecular bone changes before tooth extraction (at 4 weeks). E, F. Trabecular bone changes after tooth extraction (at 12 weeks). Bone is shown in light blue, while bone space is shown in red in B, C, E, and F.

extraction site were selected, and the BFV was measured using the MRA images in 3D Synapse software (Figs. 4A-C). BFV estimation was attained by calculating the displacement of blood between 2 consecutive images and determining the blood velocity using the fused images. An ROI consisting of the closest artery and its branch connect-

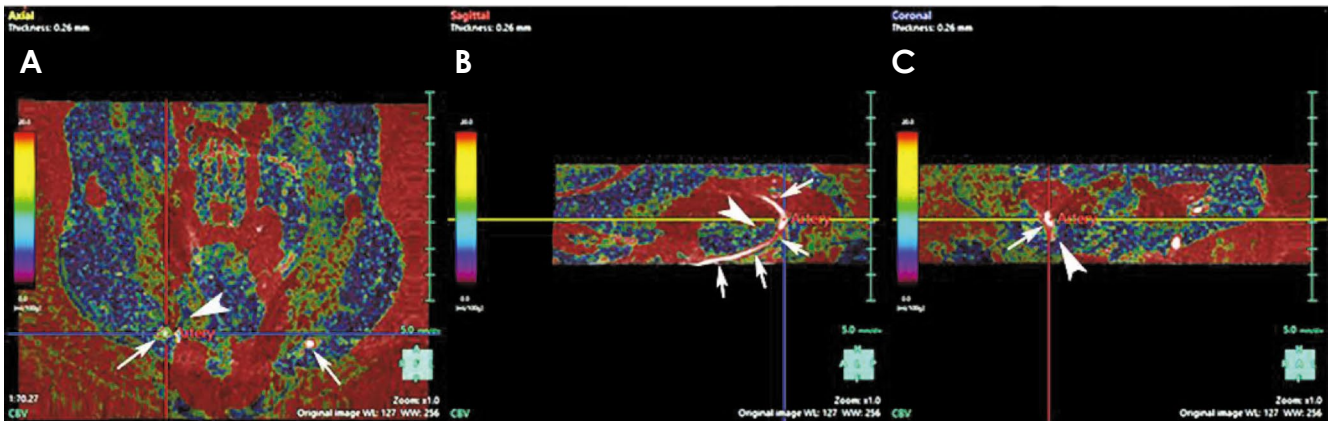

Fig. 4. Calculation of relative blood flow velocity using dedicated 3-dimensional software. A. Superimposed time-of-flight magnetic resonance angiography (TOF-MRA) and micro-computed tomography (micro-CT) images. The base image is a micro-CT scan, and the fused image is a TOF-MRA scan. B, C. The arrows denote the artery and its part connected to the tooth extraction site, while arrowheads denote the mandibular trabecular bone, coded in blue.

ed to the extraction site with dimensions of 1 × 1 pixels was selected to calculate the average velocity in the sagittal and coronal sections. The gray-level image intensity values of the artery's interior, acquired from the TOF-MRA ROIs, were used to estimate the relative BFV. The relative velocity values were then linearly fitted to the reference values. All measurements were converted to pixels/s. A single experienced observer performed the image registration and evaluation at all time points (from T0 to T20). The calculated BFV distribution was visualized using color-coding on the fused images.

Histological analysis

Histological assessment was the gold standard with which the findings were compared. All rats were sacrificed immediately after the T20 micro-CT and HR-MRI scans. Following euthanasia of all rats with an overdose of general anesthesia (1.5%-2% isoflurane in 100% oxygen), the mandibles were harvested, fixed in buffered formalin (pH 7.4), and embedded in paraffin blocks. The bone samples were decalcified under controlled slow oscillations in a 1:1 solution of 4% formic acid and 10% neutral buffered formaldehyde at a pH of 7.4 for 4 days; following demineralization, the samples were rinsed with distilled water. A single 6-μm section of each sample parallel to the mandibular body (Fig. 5A) was stained with hematoxylin solution (Gill III; Leica Microsystems, Diegem, Belgium) and 1% aqueous eosin solution (Leica Microsystems). The histological sections were manually registered and spatially aligned with the corresponding reconstructed micro-CT and HR-MRI images for evaluation of the same region of interest.[28] Thereafter, histological assessment of blood vessels was performed using a light microscope (Axio Imager M2; Carl Zeiss Microscopy, Jena, Germany).

The data obtained in this study were analyzed with IBM SPSS Statistics version 22 (IBM Corp., Armonk, NY, USA). The Mann-Whitney *U* test was applied to compare the control and test rats, as the data were not normally distributed. When interpreting the results, 0.05 was utilized as the level of significance.

Results

The rats in the study demonstrated good hemostasis following surgery and a normal recovery from anesthesia. In all cases, micro-CT revealed broken apical root remnants after extraction due to the presence of divergence and broadening in the apical root portion. However, complete and normal mucosal healing was observed at approximately 2 weeks in all rats without any visible infection.

The micro-CT component of the registered micro-CT/HR-MRI data showed an increase in Tb.Th from baseline to T20 in both the test and control rats (Fig. 5B). However, this difference lacked significance at all time points ($P > 0.05$). The micro-CT findings were consistent with the histomorphometric analysis at T20, which revealed thicker trabecular bone and smaller marrow spaces in the test rats than in the control rat (Figs. 5C and D). Additionally, the registered HR-MRI component and 3D reconstruction of blood vessels showed a reduction in test-rat BFV (Fig. 5E) and bone vascularity (Figs. 5F and G) at the same region of interest relative to the control rat at follow-up. Although an increase in BFV was observed before tooth extraction, both control and test rats showed a decrease in BFV at

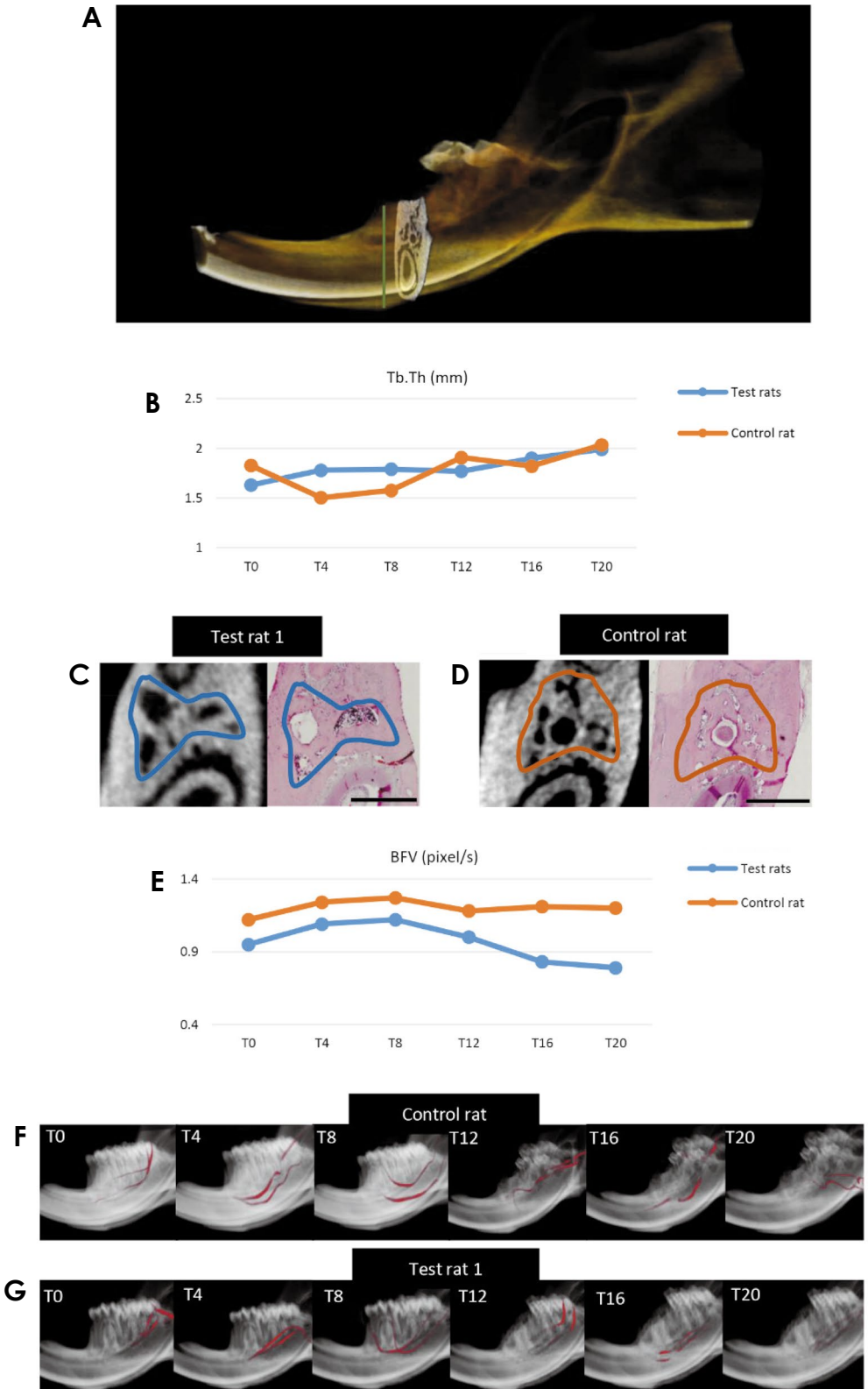

Fig. 5. Vascular and trabecular changes. A. Three-dimensional (3D) representation of the cutting direction for histological sectioning (green line: cutting plane). B. Graphical representation of changes in trabecular bone thickness in the test rats and control rat. C, D. Thicker trabecular bone and smaller marrow spaces in the micro-CT scan and histological section in a test rat compared to the control rat at T20. E. Graphical representation of BFV changes in control and test rats. F. 3D vascular changes in the control rat. G. 3D vascular changes in a test rat. BFV: blood flow velocity, Tb.Th: trabecular bone thickness, T0: baseline, T4: (4 weeks), T8: 8 weeks, T12: 12 weeks, T16: 16 weeks, and T20: 20 weeks. Bar: 1000 µm.

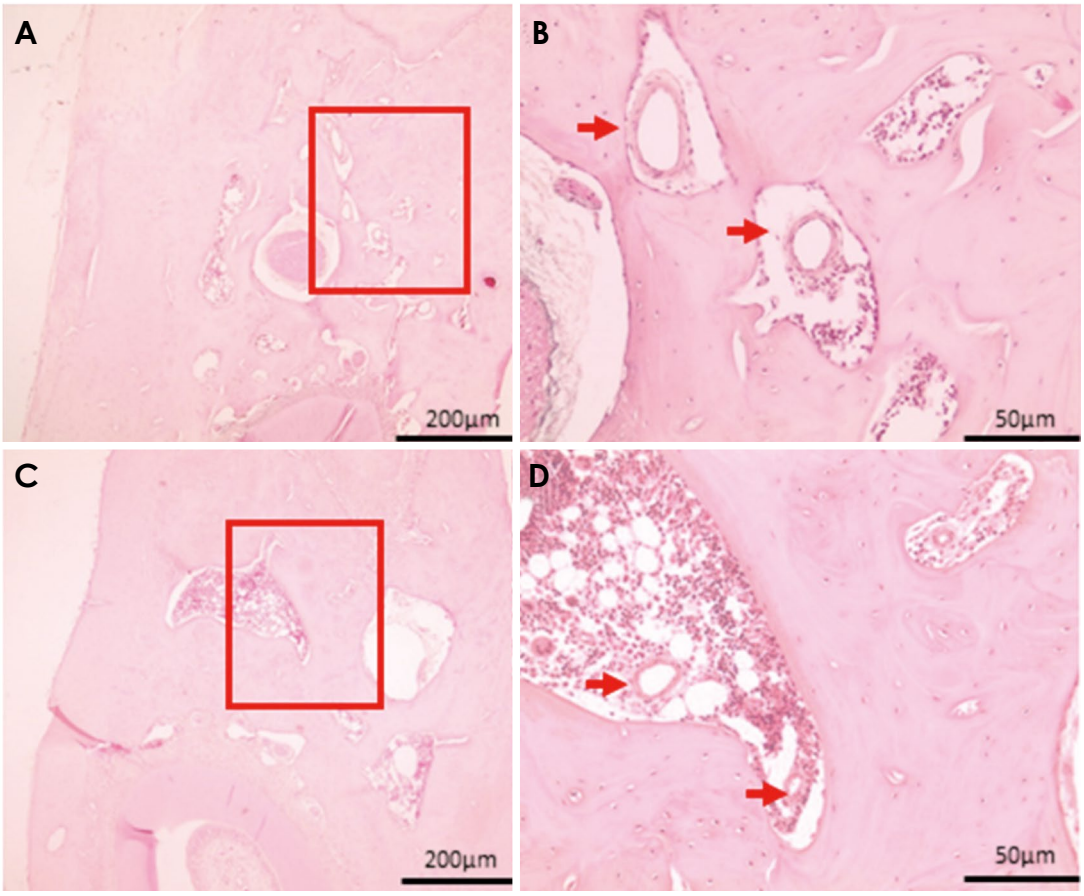

Fig. 6. Histomorphometric analysis of the blood vessels in the region of interest. A. Normal blood vessels observed in the control rat. B. Magnification of the red square in A. C. Inflamed and defective blood vessel revealed in the test rat. D. Magnification of the red square in C. Red arrow: blood vessel.

follow-up. The difference between the left and right mandibular BFV values in each rat was insignificant at all time points ($P > 0.05$). The histomorphometric images at T20 were also in accordance with the HR-MRI findings, as they demonstrated reduced trabecular bone vasculature and blood vessel density in both test and control rats and thereby confirmed the reduction in BFV. Histomorphometric analysis further revealed the presence of normal and healthy blood vessels in the control rat (Figs. 6A and B), whereas inflamed and smaller blood vessels were observed in the test rats (Figs. 6C and D). These findings were also consistent with the HR-MRI images, which revealed a greater reduction in BFV in the test rats than in the control rat based on the presence of less dense blood vessels.

Discussion

The high mineralization of human jaw bone is linked to its local vascularity.[31] Furthermore, the skeletal vasculature plays an important role in providing nutrients to bone, and any alteration in vascularization can directly influence skeletal metabolic activity and remodeling.[32] Bone disorders such as osteoporosis, rheumatoid arthritis, BRONJ, and other skeletal disorders are known to create imbalance in the remodeling process, thereby influencing the structural and functional integrity of bone and blood vessels[33]. Therefore, in the present study, a multimodal imaging technique involving a combination of micro-CT and HR-MRI was utilized for the 3D visualization, quantification, and longitudinal monitoring of bone remodeling and BFV in a BRONJ-like defect. To the best of our knowledge, a multimodal technique that can effectively and concomitantly assess bone remodeling and vascularity at follow-up has not yet been reported.

Previous studies have demonstrated the estimation of vascularization via perfusion imaging involving HR-MRI and dynamic contrast imaging techniques.[34-36] However, the disadvantages of perfusion imaging include the confu-

sion or omission of microstructure resulting from low spatial resolution. Additionally, numerous micro-CT protocols involving vascular contrast agents have also been applied to assess blood vessels, but they cannot be used to accurately assess the microvasculature.[14,28] Therefore, in this study, we utilized HR-MRI, which allows assessment of vascular structures and BFV at the microscopic level without the need for histological sectioning and staining.[37] As part of this technique, we evaluated the vascularity changes utilizing TOF-MRA, which is a common method for clinical blood vessel examination and blood flow imaging. The utilization of HR-MRI for the microanatomical and neurovascular assessment of the mandibular incisive canal,[38] nasopalatine canal, and superior and inferior genial spinal foramina[39,40] has been extensively reported. The combination of HR-MRI with micro-CT as a gold standard for bone morphometry allowed for the accurate determination of trabecular structural changes and BFV in the same region of interest.

Batise et al.[41] co-registered HR-MRI and micro-CT datasets in an *ex vivo* rabbit anterior cruciate ligament transection model and confirmed the successful application of this method in accurately quantifying the localized changes in both soft and hard tissue. However, the authors failed to quantify changes at follow-up. Other studies have involved the co-registration of micro-CT and MRI datasets for the assessment of bone and vascular changes; however, the application of MRI is limited based on low spatial resolution and the inability to provide detailed information related to microvascular structures in animal studies.[23,24] In contrast, our methodology allowed accurate quantification of both bone microstructure and blood vessels in the test and control rats at follow-up, suggesting that a combination of HR-MRI and micro-CT may provide a reasonable means to monitor the localized progression of ONJ in a preclinical rat model.

The combination of different imaging modalities provided localization and distinction of mineralization and vascularization in the mandible. The changes in trabecular bone and vascularity were assessed in the same ROI, and our findings associated with bone remodeling were consistent with the results of the histomorphometric analysis. We observed localized mineralization and a reduction in vascularization with smaller marrow spaces and narrow canals, which were in accordance with the previous findings.[28,42,43]

It should be mentioned that based on the small sample size, significant evidence regarding the interaction of bone vascularization and remodeling could not be found. Further prospective studies utilizing a similar methodology should thus be carried out with a larger sample size to confirm our findings. It is also recommended to explore the potential of adding a contrast medium, so as to focus on possible beneficial effects for co-registered imaging of vascularization and bone remodeling.

In conclusion, the combination of micro-CT and HR-MRI may be considered a powerful non-invasive tool for the longitudinal concomitant quantification of bone remodeling and vascularization. The present protocol should be further applied and validated with an integrated animal experimental design.

Conflicts of Interest: None

References

1. Maes C. Role and regulation of vascularization processes in endochondral bones. Calcif Tissue Int 2013; 92: 307-23.
2. Driessens M. Circulatory aspects of reflex sympathetic dystrophy. In: Schoutens A, Gardeniers JW, Hughes SP. Bone circulation and vascularization in normal and pathological conditions. New York: Springer; 1993. p. 217-31.
3. Boerckel JD, Uhrig BA, Willett NJ, Huebsch N, Guldberg RE. Mechanical regulation of vascular growth and tissue regeneration in vivo. Proc Natl Acad Sci U S A 2011; 108: E674-80.
4. Eghbali-Fatourechi GZ, Mödder UI, Charatcharoenwitthaya N, Sanyal A, Undale AH, Clowes JA, et al. Characterization of circulating osteoblast lineage cells in humans. Bone 2007; 40: 1370-7.
5. Ishii M, Egen JG, Klauschen F, Meier-Schellersheim M, Saeki Y, Vacher J, et al. Sphingosine-1-phosphate mobilizes osteoclast precursors and regulates bone homeostasis. Nature 2009; 458: 524-8.
6. Thompson B, Towler DA. Arterial calcification and bone physiology: role of the bone-vascular axis. Nat Rev Endocrinol 2012; 8: 529-43.
7. Mark H, Penington A, Nannmark U, Morrison W, Messina A. Microvascular invasion during endochondral ossification in experimental fractures in rats. Bone 2004; 35: 535-42.
8. Deshpande SS, Donneys A, Farberg AS, Tchanque-Fossuo CN, Felice PA, Buchman SR. Quantification and characterization of radiation-induced changes to mandibular vascularity using micro-computed tomography. Ann Plast Surg 2014; 72: 100-3.
9. Prajapati SI, Keller C. Contrast enhanced vessel imaging using microCT. J Vis Exp 2011; 47: 2377.
10. Abma E, Stock E, De Spiegelaere W, Van Brantegem L, Vanderperren K, Ni Y, et al. Power Doppler ultrasound and contrast-enhanced ultrasound demonstrate non-invasive tumour vascular response to anti-vascular therapy in canine cancer patients. Sci Rep 2019; 9: 9262.
11. Hillier ML, Bell LS. Differentiating human bone from animal bone: a review of histological methods. J Forensic Sci 2007;

52: 249-63.
12. Jorgensen SM, Demirkaya O, Ritman EL. Three-dimensional imaging of vasculature and parenchyma in intact rodent organs with X-ray micro-CT. Am J Physiol 1998; 275: H1103-14.
13. Yang J, Pham SM, Crabbe DL. High-resolution micro-CT evaluation of mid-to long-term effects of estrogen deficiency on rat trabecular bone. Acad Radiol 2003; 10: 1153-8.
14. Fei J, Peyrin F, Malaval L, Vico L, Lafage-Proust MH. Imaging and quantitative assessment of long bone vascularization in the adult rat using microcomputed tomography. Anat Rec (Hoboken) 2010; 293: 215-24.
15. Roche B, David V, Vanden-Bossche A, Peyrin F, Malaval L, Vico L, et al. Structure and quantification of microvascularisation within mouse long bones: what and how should we measure? Bone 2012; 50: 390-9.
16. Weinstein RS, Wan C, Liu Q, Wang Y, Almeida M, O'Brien CA, et al. Endogenous glucocorticoids decrease skeletal angiogenesis, vascularity, hydration, and strength in aged mice. Aging Cell 2010; 9: 147-61.
17. Ding WG, Wei ZX, Liu JB. Reduced local blood supply to the tibial metaphysis is associated with ovariectomy-induced osteoporosis in mice. Connect Tissue Res 2011; 52: 25-9.
18. Barentsz JO, Engelbrecht M, Jager GJ, Witjes JA, de LaRosette J, van der Sanden BP, et al. Fast dynamic gadolinium-enhanced MR imaging of urinary bladder and prostate cancer. J Magn Reson Imaging 1999; 10: 295-304.
19. Benjaminsen IC, Graff BA, Brurberg KG, Rofstad EK. Assessment of tumor blood perfusion by high-resolution dynamic contrast-enhanced MRI: a preclinical study of human melanoma xenografts. Magn Reson Med 2004; 52: 269-76.
20. Zagorchev L, Oses P, Zhuang ZW, Moodie K, Mulligan-Kehoe MJ, Simons M, et al. Micro computed tomography for vascular exploration. J Angiogenes Res 2010; 2: 7.
21. Liang H, Yang Y, Yang K, Wu Y, Boone JM, Cherry SR. A microPET/CT system for in vivo small animal imaging. Phys Med Biol 2007; 52: 3881-94.
22. Bernsen MR, Vaissier PE, Van Holen R, Booij J, Beekman FJ, de Jong M. The role of preclinical SPECT in oncological and neurological research in combination with either CT or MRI. Eur J Nucl Med Mol Imaging 2014; 41 Suppl 1: S36-49.
23. Kłodowski K, Kamiński J, Nowicka K, Tarasiuk J, Wroński S, Swiętek M, et al. Micro-imaging of implanted scaffolds using combined MRI and micro-CT. Comput Med Imaging Graph 2014; 38: 458-68.
24. Basha MA, AlAzzazy MZ, Ahmed AF, Yousef HY, Shehata SM, El Sammak DA, et al. Does a combined CT and MRI protocol enhance the diagnostic efficacy of LI-RADS in the categorization of hepatic observations? A prospective comparative study. Eur Radiol 2018; 28: 2592-603.
25. Lin MT, Wang CC, Cheng YF, Eng HL, Yen YH, Tsai MC, et al. Comprehensive comparison of multiple-detector computed tomography and dynamic magnetic resonance imaging in the diagnosis of hepatocellular carcinoma with varying degrees of fibrosis. PLoS One 2016; 11: e0166157.
26. Badea CT, Hedlund LW, De Lin M, Boslego Mackel JF, Johnson GA. Tumor imaging in small animals with a combined micro-CT/micro-DSA system using iodinated conventional and blood pool contrast agents. Contrast Media Mol Imaging 2006; 1: 153-64.
27. Longo AB, Sacco SM, Ward WE. Proper positioning and restraint of a rat hind limb for focused high resolution imaging of bone micro-architecture using in vivo micro-computed tomography. J Vis Exp 2017; 129: 56346.
28. Soares MQ, Van Dessel J, Jacobs R, da Silva Santos PS, Cestari TM, Garlet GP, et al. Zoledronic acid induces site-specific structural changes and decreases vascular area in the alveolar bone. J Oral Maxillofac Surg 2018; 76: 1893-901.
29. Sharma D, Hamlet S, Petcu E, Ivanovski S. Animal models for bisphosphonate-related-osteonecrosis of the jaws - an appraisal. Oral Dis 2013; 19: 747-54.
30. Huang TC, Chang CK, Liao CH, Ho YJ. Quantification of blood flow in internal cerebral artery by optical flow method on digital subtraction angiography in comparison with time-of-flight magnetic resonance angiography. PLoS One 2013; 8: e54678.
31. Faot F, Chatterjee M, de Camargos G, Duyck J, Vandamme K. Micro-CT analysis of the rodent jaw bone micro-architecture: a systematic review. Bone Rep 2015; 2: 14-24.
32. Siddiqui JA, Partridge NC. Physiological bone remodeling: systemic regulation and growth factor involvement. Physiology (Bethesda) 2016; 31: 233-45.
33. Bamias A, Kastritis E, Bamia C, Moulopoulos LA, Melakopoulos I, Bozas G. Osteonecrosis of the jaw in cancer after treatment with bisphosphonates: incidence and risk factors. J Clin Oncol 2005; 23: 8580-7.
34. Principi M, Italiani M, Guiducci A, Aprile I, Muti M, Giulianelli G, et al. Perfusion MRI in the evaluation of the relationship between tumour growth, necrosis and angiogenesis in glioblastomas and grade 1 meningiomas. Neuroradiology 2003; 45: 205-11.
35. Law M, Cha S, Knopp EA, Johnson G, Arnett J, Litt AW. High-grade gliomas and solitary metastases: differentiation by using perfusion and proton spectroscopic MR imaging. Radiology 2002; 222: 715-21.
36. Lee SJ, Kim JH, Kim YM, Lee GK, Lee EJ, Park IS, et al. Perfusion MR imaging in gliomas: comparison with histologic tumor grade. Korean J Radiol 2001; 2: 1-7.
37. Vandersteen M, Beuls E, Gelan J, Adriaensens P, Vanormelingen L, Palmers Y, et al. High field magnetic resonance imaging of normal and pathologic human medulla oblongata. Anat Rec 1994; 238: 277-86.
38. Jacobs R, Lambrichts I, Liang X, Martens W, Mraiwa N, Adriaensens P, et al. Neurovascularization of the anterior jaw bones revisited using high-resolution magnetic resonance imaging. Oral Surg Oral Med Oral Pathol Oral Radiol Endod 2007; 103: 683-93.
39. Kress B, Gottschalk A, Anders L, Stippich C, Palm F, Bähren W, et al. High-resolution dental magnetic resonance imaging of inferior alveolar nerve responses to the extraction of third molars. Eur Radiol 2004; 14: 1416-20.
40. Du Tolt DF, Nortjé C. The maxillae: integrated and applied anatomy relevant to dentistry. SADJ 2003; 58: 325-30.
41. Batiste DL, Kirkley A, Laverty S, Thain LM, Spouge AR,

Gati JS, et al. High-resolution MRI and micro-CT in an ex vivo rabbit anterior cruciate ligament transection model of osteoarthritis. Osteoarthritis Cartilage 2004; 12: 614-26.
42. Kün-Darbois JD, Libouban H, Mabilleau G, Pascaretti-Grizon F, Chappard D. Bone mineralization and vascularization in bisphosphonate-related osteonecrosis of the jaw: an experimental study in the rat. Clin Oral Investig 2018; 22: 2997-3006.
43. Bi Y, Gao Y, Ehirchiou D, Cao C, Kikuiri T, Le A, et al. Bisphosphonates cause osteonecrosis of the jaw-like disease in mice. Am J Pathol 2010; 177: 280-90.